

PAPER • OPEN ACCESS

Primary Si refinement and eutectic Si modification in Al-20Si via P-Ce addition

To cite this article: Peerawit Chokemorn *et al* 2022 *Mater. Res. Express* **9** 036501

View the [article online](#) for updates and enhancements.

You may also like

- [Microstructural characteristics and evolution of *in situ* xTiB₂/Al-20%Si alloy](#)
Ying Xiao, Lu Li, Qiuping Wang et al.
- [Effect of particle size on the microstructure and tensile property of the Al-28.5Si alloy prepared by continuous powder extrusion](#)
Jiancheng Yin, Yanfei Li, Yingshuo Niu et al.
- [Modification of multi-component Al-Si casting piston alloys by addition of rare earth yttrium](#)
Qinglin Li, Shang Zhao, Binqiang Li et al.



PAPER

Primary Si refinement and eutectic Si modification in Al-20Si via P-Ce addition

OPEN ACCESS

RECEIVED

14 February 2022

REVISED

23 February 2022

ACCEPTED FOR PUBLICATION

25 February 2022


PUBLISHED

9 March 2022

Original content from this work may be used under the terms of the [Creative Commons Attribution 4.0 licence](https://creativecommons.org/licenses/by/4.0/).

Any further distribution of this work must maintain attribution to the author(s) and the title of the work, journal citation and DOI.



Peerawit Chokemorh¹, Phromphong Pandee^{1,2}, Suwaree Chankitmunkong³, Ussadawut Patakham⁴ and Chaowalit Limmaneevichitr¹ 

¹ Department of Production Engineering, Faculty of Engineering, King Mongkut's University of Technology Thonburi, Bangmod, Tungkhru, Bangkok 10140, Thailand

² Center for Lightweight Materials, Design and Manufacturing, King Mongkut's University of Technology Thonburi, Bangmod, Tungkhru, Bangkok 10140, Thailand

³ Department of Industrial Engineering, School of Engineering, King Mongkut's Institute of Technology Ladkrabang, Ladkrabang, Bangkok 10520, Thailand

⁴ National Metal and Material Technology Center, National Sciences and Technology Development Agency, Thailand Science Park, Klong Luang, Pathumthani 12120, Thailand

E-mail: chaowalit.lim@mail.kmutt.ac.th

Keywords: hypereutectic Al-Si, cerium, eutectic silicon, primary silicon, wear, rare earth

Abstract

Enhancing the mechanical properties of hypereutectic Al-Si alloys by refining the primary and eutectic Si morphology is very challenging. In this study, the refinement mechanism of primary and eutectic Si morphologies via the simultaneous addition of P-Ce into the Al-20Si alloy was studied.

Microstructural analysis revealed that the primary and eutectic Si morphologies were significantly refined, which increased the tensile strength. Furthermore, the addition of Ce, up to 0.6 wt%, can result in the formation of Ce-rich intermetallic phases, which may lead to a significantly increased tensile strength while retaining the ductility of the alloy. The ultimate tensile strength of the Al-20Si alloy increased from 96 to 175 MPa, and the elongation increased from 1.0% to 1.7% with the addition of P-Ce. Moreover, the wear resistance of the alloy improved. The added P and Ce did not react with each other to form an intermetallic compound; therefore, this method can simultaneously refine primary and eutectic Si.

1. Introduction

Hypereutectic Al-Si alloys are widely used in the automotive and aerospace industries because of their excellent tribological performance in high-operating-temperature applications. The occurrence of a hard phase of primary Si that precipitates during solidification leads to the excellent wear resistance of the alloy, which depends on the structure of the primary Si and its distribution in the matrix. Moreover, the presence of large and unevenly distributed primary Si particles decreases the lifespan of the machine tool. Therefore, the primary and eutectic Si structure should be refined and uniformly distributed to minimize the excessive wear of the machine tool and achieve adequate tensile strength and other desirable properties.

Phosphorus is an effective refiner for hypereutectic Al-Si alloys [1]. The addition of P forms aluminum phosphide (AlP), which acts as a heterogeneous nucleus for primary Si, resulting in the reduced size and good dispersion of the primary Si phase [2, 3]. The best refinement of primary Si occurs at 0.003–0.006 wt% P, which decreases the primary Si size to approximately 20 μm [1]. However, P does not affect the modification of eutectic Si, which retains its coarse acicular morphology [4]. Sr and Na effectively modify the eutectic Si phase from a coarse, needle-like structure to a fine fibrous morphology [5, 6]. However, in hypereutectic Al-Si alloys, it is very difficult to refine primary and eutectic Si via the simultaneous addition of P and conventional modifiers. This may be because of the mutual interaction between P and the modifying elements [5, 7].

Previous research has established that rare earth elements can refine primary Si and modify eutectic Si, thereby improving the mechanical properties [8–12]. However, the mechanisms by which rare earth elements

affect the primary and eutectic Si morphologies remain undefined and may favor either nucleation or growth. Among the various available rare earth elements, Ce is a good candidate for microalloying in Al-Si casting alloys because of its comparably low cost. Several studies have been performed to determine the effect of Ce addition on hypereutectic Al-Si alloys [10–12]. Li *et al* [10] reported that the addition of Ce can significantly refine primary Si and modify eutectic Si. Chang *et al* [13] concluded that the primary Si morphology was altered from a star-shaped to fine polyhedral structure. However, Weiss and Loper [14] suggested that the addition of Ce had no refining effect on the primary Si crystal compared with the addition of P. Therefore, the refinement mechanism of primary and eutectic Si via Ce addition, together with P, remains unclear. Moreover, our previous study demonstrated that the addition of Sc to Al-20Si alloys does not refine the primary Si because Sc decreases the P refinement efficiency by forming ScP, resulting in the less active P to form AlP, which is an effective nucleation site for the primary Si phase [15].

The primary Si refinement mechanisms are normally elucidated according to nucleation and growth theories. Primary Si nuclei grow from Si-Si atom clusters that exist in the melt above the liquidus temperature [16]. To refine primary Si, heterogeneous nucleation with a cube-cube orientation relationship has been conducted via the addition of P to form AlP particles that can act as the nucleation substrate [2, 17]. Furthermore, the twin plane re-entrant edge (TPRE) growth mechanism has been employed to explain the growth of the primary Si [18, 19]. Increasing twin formation with multi-orientation variations leads to primary Si refinement. Restricted nucleation and growth theories have been proposed to elucidate the mechanisms of the eutectic Si modification. Restricted nucleation theories are based on the fact that modifier elements react with preexisting nuclei in the melt and reduce the nucleation events of eutectic Si [20]. According to the restricted growth theory, modifier atoms adsorb on the TPRE sites of growing Si crystals and slow the growth of eutectic Si [21].

In this study, the potential of P and Ce as complex modifying agents for the simultaneous refinement of primary and eutectic Si in hypereutectic Al-20Si alloys was investigated. The mutual effects of the P-Ce addition on the microstructure, mechanical properties, and wear resistance properties were also examined. The present study helps to determine the possible use of Ce in hypereutectic Al-Si alloys without experiencing the poisoning effect of P.

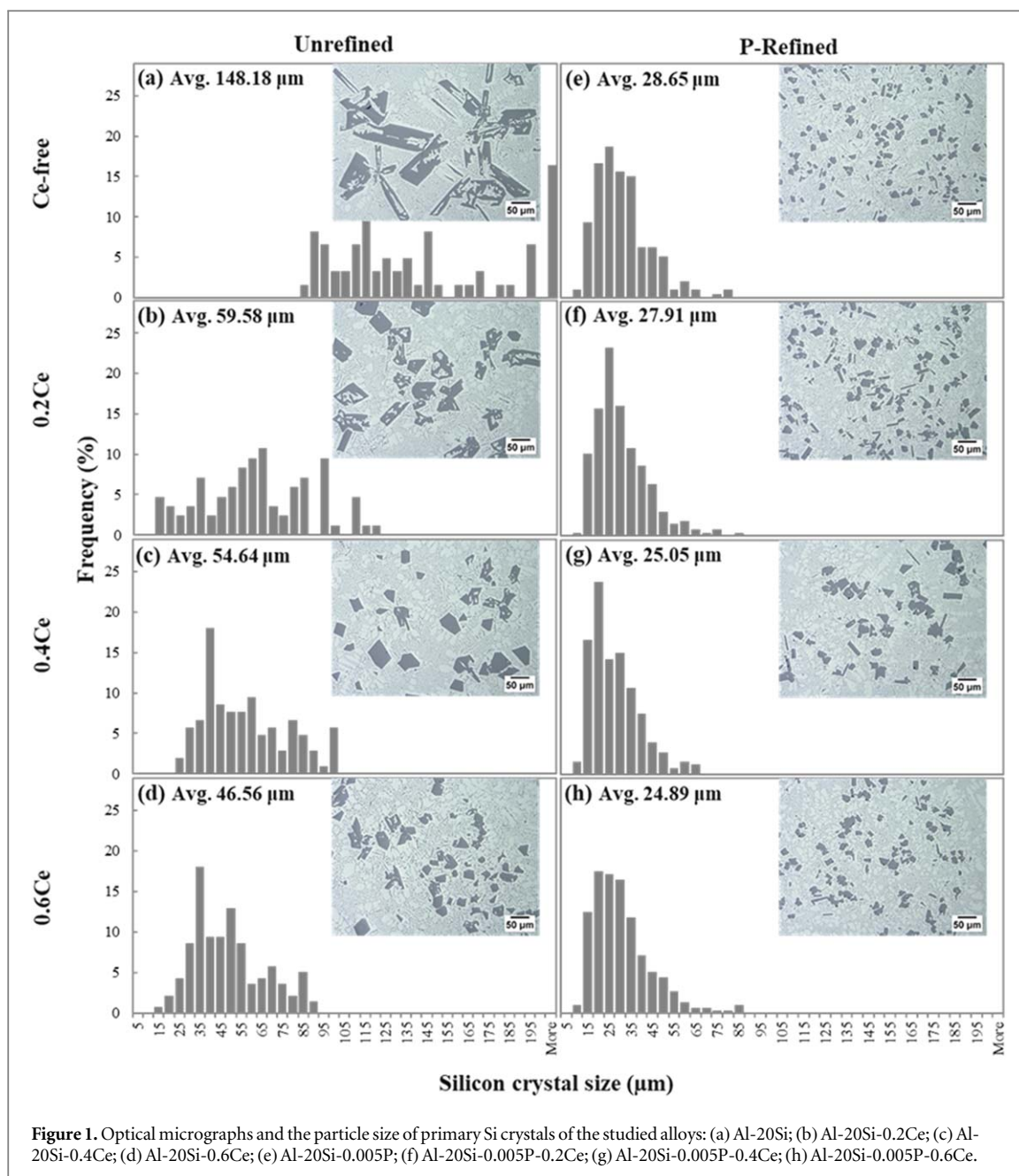
2. Materials and methods

The composition of the base alloy used in the present study was 20.28 wt% Si, 0.017 wt% Cu, 0.256 wt% Fe, and the remainder Al (wt% is used throughout the article unless otherwise stated). Commercially pure 99.7% Al and 99.0% Si were used to prepare the base alloys. The Al-20Si alloy was subsequently remelted at 800 °C in an induction furnace. Thereafter, Al-5wt% P and Al-10wt% Ce were added at 800 °C to produce eight sets of Al-20Si alloys: Al-20Si, Al-20Si-0.2Ce, Al-20Si-0.4Ce, Al-20Si-0.6Ce, Al-20Si-0.005P, Al-20Si-0.005P-0.2Ce, Al-20Si-0.005P-0.4Ce, and Al-20Si-0.005P-0.6Ce. The melt was maintained for at least 15 min at 800 °C to ensure its homogeneity. Argon was purged into the bottom of the crucible through a stainless-steel tube, and the dross was carefully skimmed. The alloy melt at 750 °C was poured into a copper mold with a length of 170 mm and a diameter of 20 mm at room temperature. The samples were cut 20 mm above the bottom, and standard metallographic techniques were used. The microstructures were observed and analyzed using an optical microscope. The primary Si crystal size (μm) was measured using the ImageJ software. Moreover, the shape factors of the primary and eutectic Si particles were calculated as follows:

$$S = \frac{\sum_{i=1}^n A_i (2\sqrt{\pi A_i} / P_i)}{\sum_{i=1}^n A_i} \quad (1)$$

where S is the mean shape factor of the Si phase; A_i is the area (μm^2) of the Si particles; P_i is the perimeter (μm) of the Si particles. This analytical technique has been previously used by several investigators to quantify the geometry of primary and eutectic Si particles [22]. The shape factor has a value of one for a perfectly round shape and less than one when the particles are irregular. Furthermore, the microstructures were analyzed using scanning electron microscopy (SEM, Thermo Scientific Apreo S and Hitachi model S-3400 N) equipped with energy-dispersive x-ray spectroscopy (EDS) and an electron backscatter diffraction (EBSD) detector. The EDAX Revision 5.0 and TSL OIM Data Collection 5.3 software were used to interpret the results obtained by the EBSD analyses. For quantitative analysis, boundaries of misorientation ranging between 1° and 15° were considered low-angle boundaries and those of higher misorientation were considered high-angle boundaries.

For thermal analysis, it is difficult to calculate the solidification parameter, which is defined as the primary Si crystallization reaction temperature at a high cooling rate. Consequently, another set of experiments were performed with a very slow cooling rate, as described in the literature [23]. The primary Si reaction temperatures for all alloys were calculated from the obtained cooling curve.

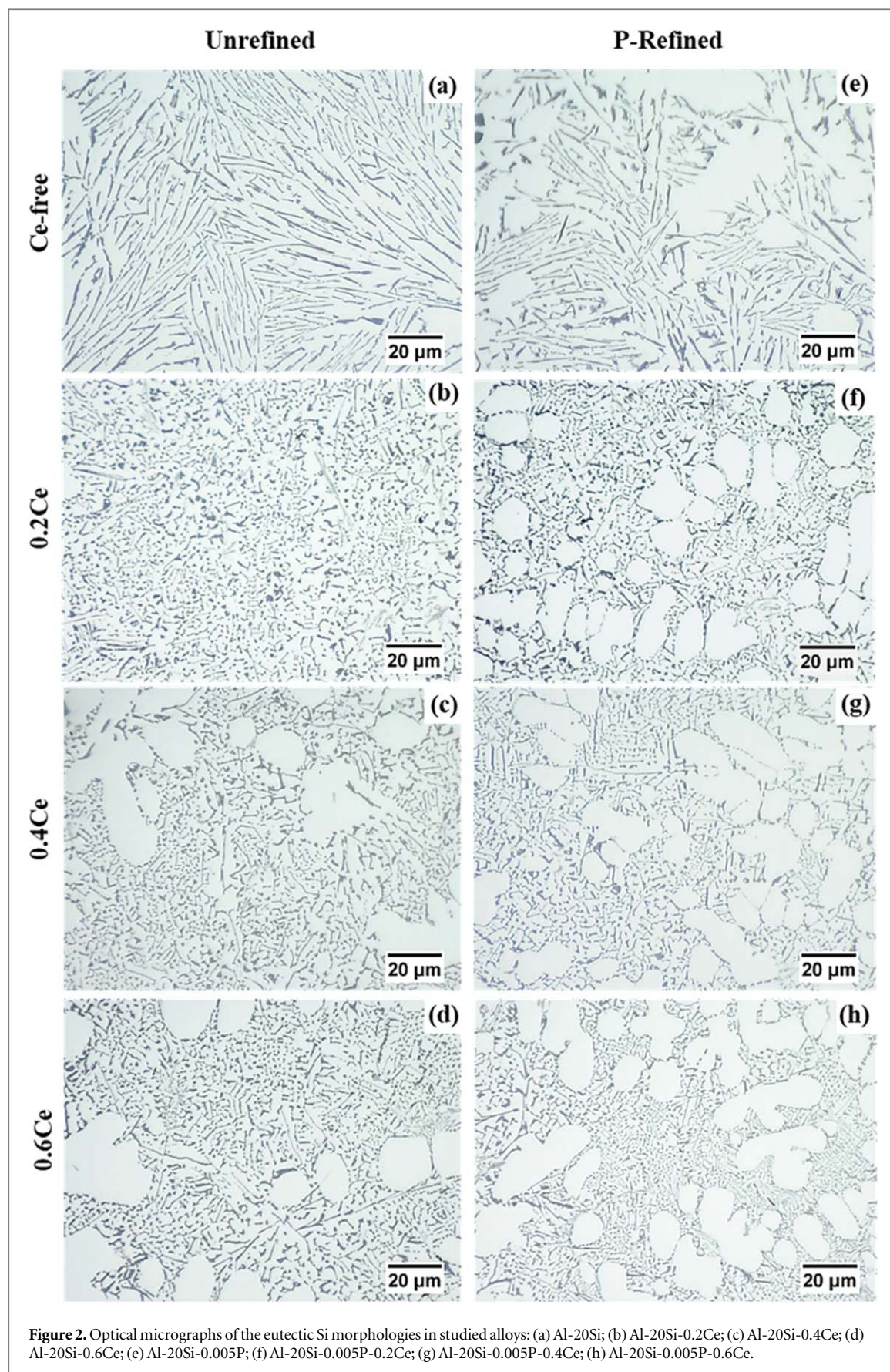


The specimens were machined to form round tensile samples, in accordance with ASTM-B557M standards. The tensile tests were performed at 25 °C at a constant tension speed of 1 mm min⁻¹. The ultimate tensile strength, yield strength, and percentage of elongation at break of the three specimens were calculated for each composition. Wear samples with diameters of 20 mm and heights of 5 mm were cut from the as-cast specimens. Ball-on-disk sliding wear tests were performed without lubrication. A sliding speed of 0.04 m s⁻¹ was used, and the samples were slid for approximately 200 m at 25 °C. The wear tests were conducted with a load of 3 N using a 6 mm diameter tungsten carbide ball. The mass of each sample was recorded before and after each test. Moreover, the tensile fracture surfaces and worn surfaces were observed and analyzed using SEM.

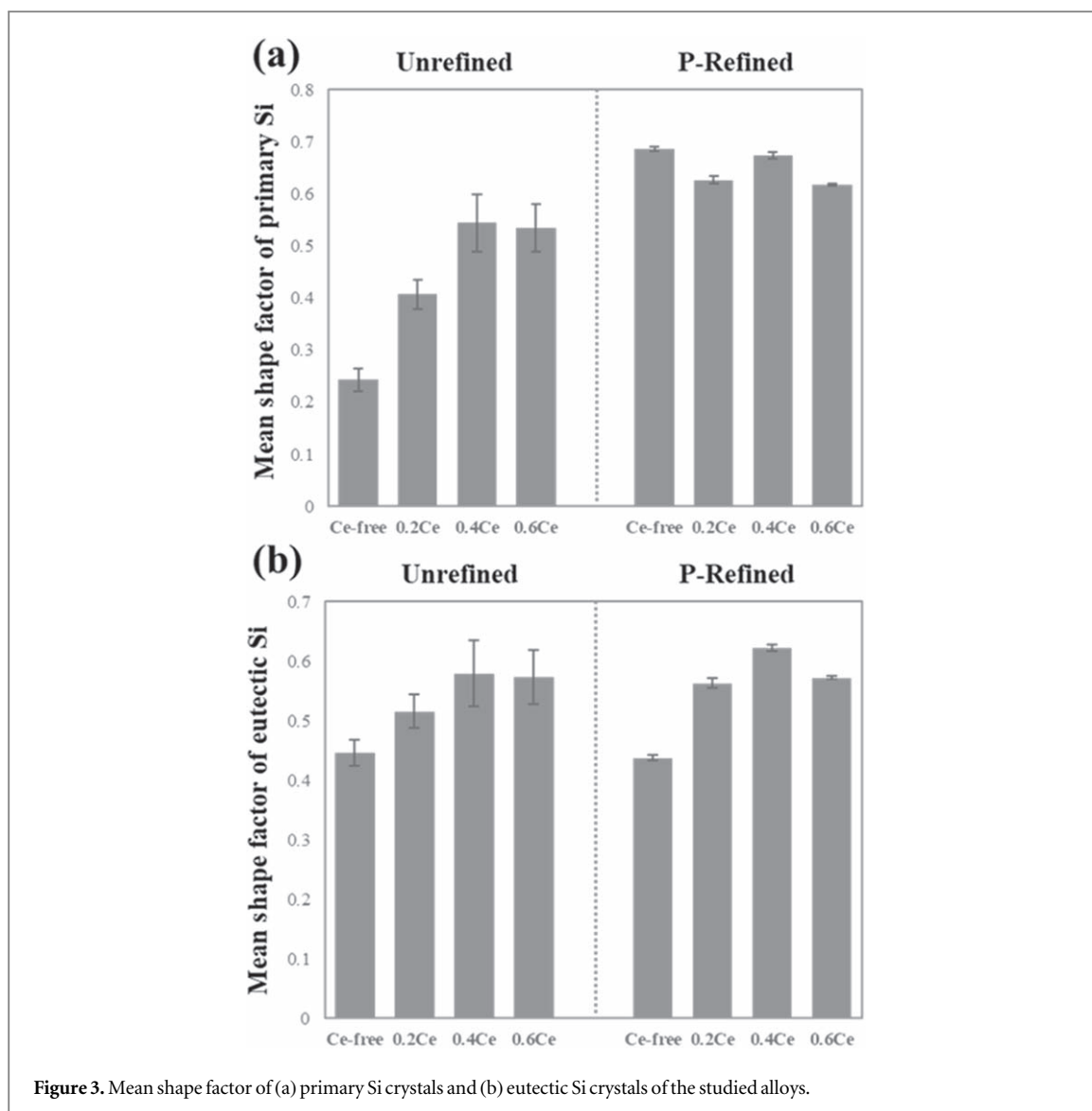
3. Results and discussion

3.1. Microstructural observation and thermal analysis

The microstructure of the Al-20Si alloy (figure 1(a)) clearly comprises of a coarse, irregular, and star-like primary Si phase. The maximum particle size was 345 μm (figure 1(a)). The morphology of the primary Si crystal changed to a polyhedral structure upon the addition of Ce (figures 1(b)–(d)). The average particle size of primary Si was reduced, and the mean shape factor of primary Si (figure 3(a)) was significantly increased by the addition of Ce. However, the refining effect of Ce on the microstructure was non-uniform. Some primary Si crystals



continued to possess an irregular shape. In the P-refined alloy (figure 1(e)), the primary Si crystal has a polyhedral shape with an average particle size of $\sim 29 \mu\text{m}$. The addition of P substantially increased the mean shape factor of the primary Si. Ce addition did not significantly alter the shape of primary Si in the P-refined alloys.



The eutectic Si in the Al-20Si alloy displays a long needle shape (figure 2(a)). The eutectic Si phase does not change with the addition of P (figure 2(e)), whereas figures 2(b)–(d) show that it is finer with the addition of Ce. The addition of Ce transformed the long needle-shaped eutectic Si into a short, rod-like structure. In contrast, the eutectic Si has a needle-like structure in the Al-20Si (figure 4(a)) and P-refined alloys (figure 4(b)). Therefore, the shape of eutectic Si transforms with an increase in the Ce content (figures 4(c)–(e)). The shape factor of eutectic Si (figure 3(b)) clearly increases with the addition of Ce. However, the addition of P did not alter the mean shape factor of eutectic Si.

The EBSD orientation maps of the eutectic regions of the studied alloys are shown in figure 5. Scans were made only for eutectic Al, omitting eutectic Si and intermetallic phases. The analysis of the EBSD orientation maps for Al-20Si showed that the large eutectic Al grain (figure 5(a)) corresponded to many low-angle grain boundaries (figure 5(e)). The addition of P and/or Ce to the Al-20Si alloy caused a reduction in the eutectic grain size (figures 5(b)–(d)) and decreased the low-angle grain boundary (figures 5(f)–(h)). A backscattered electron image and the corresponding EDS mapping analysis results for the Al-20Si-0.005P-0.6Ce sample are shown in figure 6. Many intermetallic phases are observed in the eutectic Si region of the matrix. The EDS mapping analysis (figures 6(b)–(e)) shows that there are two intermetallic phases. One phase contained Al, Si, and Ce (red arrows), whereas the other phase contained Al, Si, Fe, and Ce (yellow arrow).

A comparison between the cooling curves of the base alloy and the P- and Ce-containing alloys is shown in figure 7. Only the primary Si reaction was plotted in the thermal analysis results. For clarity, the curves were offset on the time scale. The primary Si crystallization reaction temperatures were determined from the intersection of the two tangents of the derivative curve obtained before and after nucleation. Clearly, the amounts of Ce at different compositions did not significantly change the primary Si reaction temperatures. An increase of $\sim 7^\circ\text{C}$ in the primary Si reaction temperature was observed with the addition of P as a refiner.

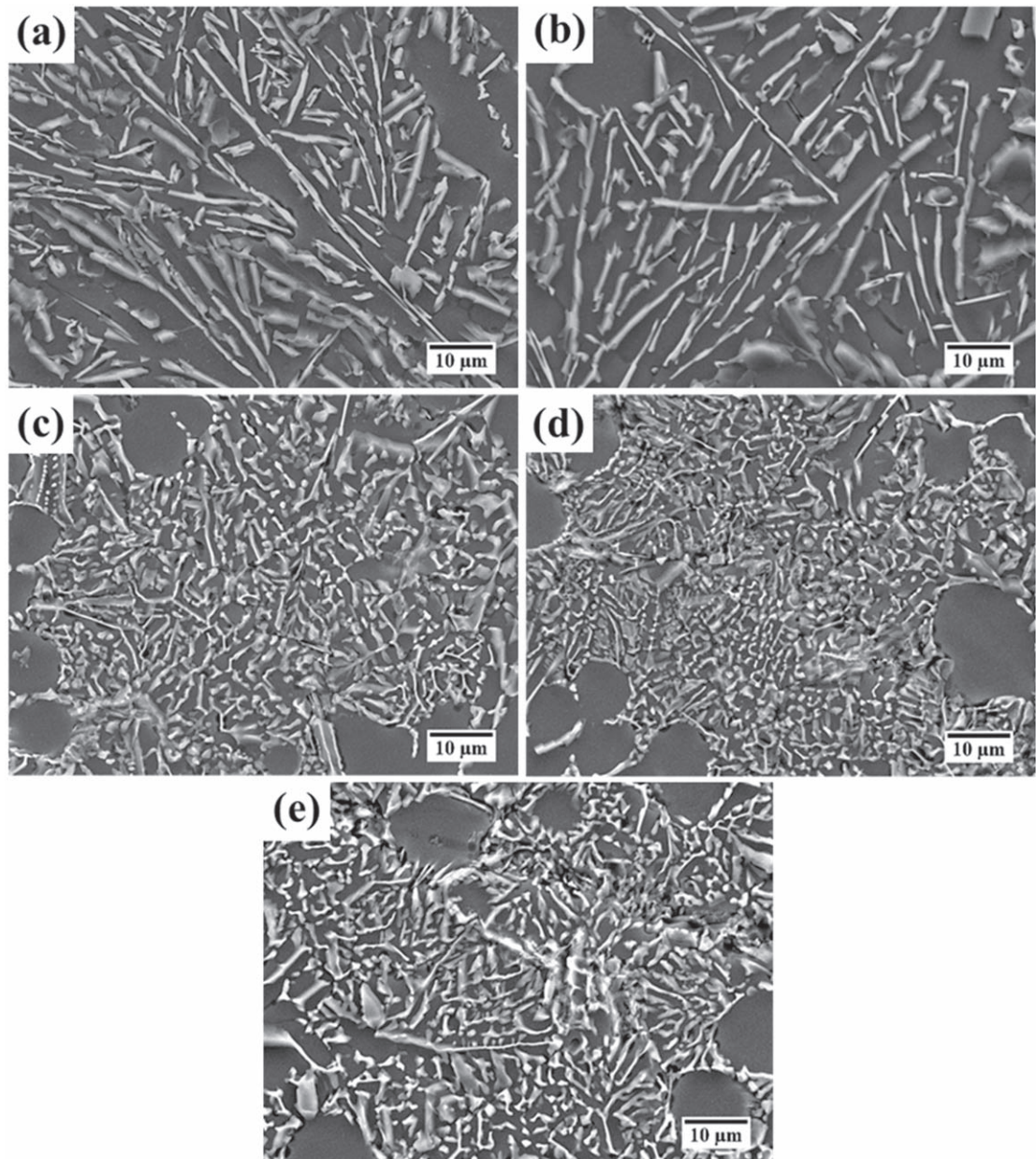


Figure 4. SEM micrographs of eutectic Si morphologies in studied alloys: (a) Al-20Si; (b) Al-20Si-0.005P; (c) Al-20Si-0.005P-0.2Ce; (d) Al-20Si-0.005P-0.4Ce; (e) Al-20Si-0.005P-0.6Ce.

3.2. Refinement mechanism of primary and eutectic Si

The addition of P refined primary Si from a coarse irregular needle- or star-like morphology to a fine polyhedral morphology (figure 1(e)). P is typically used as a chemical refiner for hypereutectic Al-Si alloys owing to the presence of AlP in the melt. In addition to the primary Si refinement, the addition of P changes the primary Si formation temperature [2]. Normally, the nucleation and growth of primary Si in a hypereutectic Al-Si alloy without P addition occurs under a high degree of undercooling. The addition of P produces a large number of AlP particles in the melt, which act as heterogeneous nuclei for primary Si nucleation [2, 3]. As a result, the addition of P forces the nucleation of primary Si to a smaller undercooling (higher nucleation temperatures). Therefore, the primary Si formation temperature increases with the addition of P.

A substantial amount of research has been conducted on the refinement effect of Ce on primary Si in hypereutectic Al-Si alloys. However, different conclusions have been reached. For instance, Chang *et al* [13] studied the effect of Ce addition on a hypereutectic Al-Si alloy and concluded that the primary Si morphology was altered from star-shaped to a fine polyhedral. However, Weiss and Loper [14] suggested that the addition of Ce had no refining effect on the primary Si crystal compared with the addition of P. Figure 1 clearly shows that the addition of Ce altered the morphology of the primary Si crystal to a polyhedral shape. Accordingly, the mechanisms of Ce and P in the refinement of primary Si are different. Chang *et al* [13] suggested that an Al-Ce

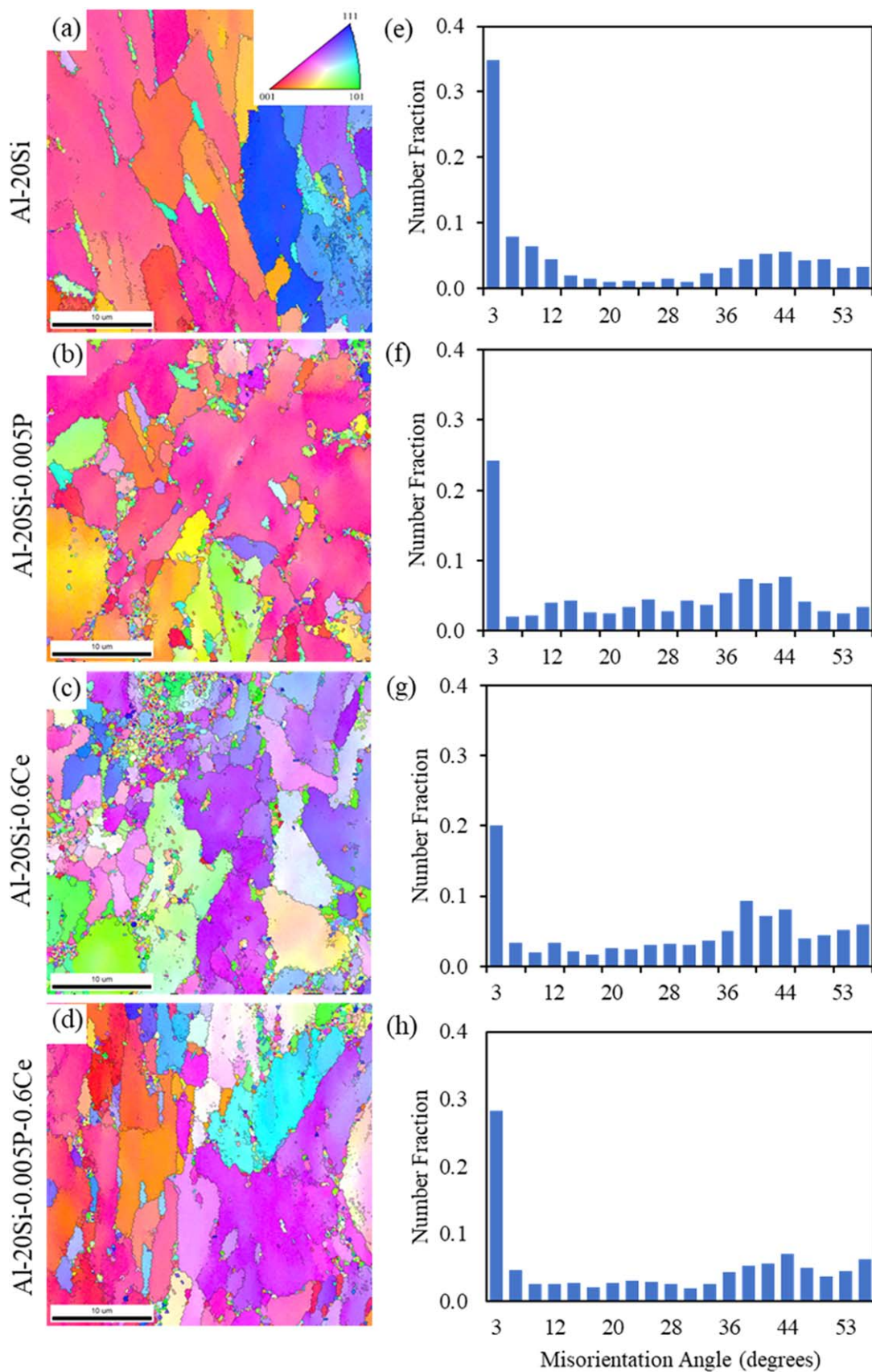


Figure 5. EBSD orientation maps and boundary misorientation distributions at the eutectic area of the samples: (a) and (e) Al-20Si; (b) and (f) Al-20Si-0.005P; (c) and (g) Al-20Si-0.6Ce; (d) and (h) Al-20Si-0.005P-0.6Ce.

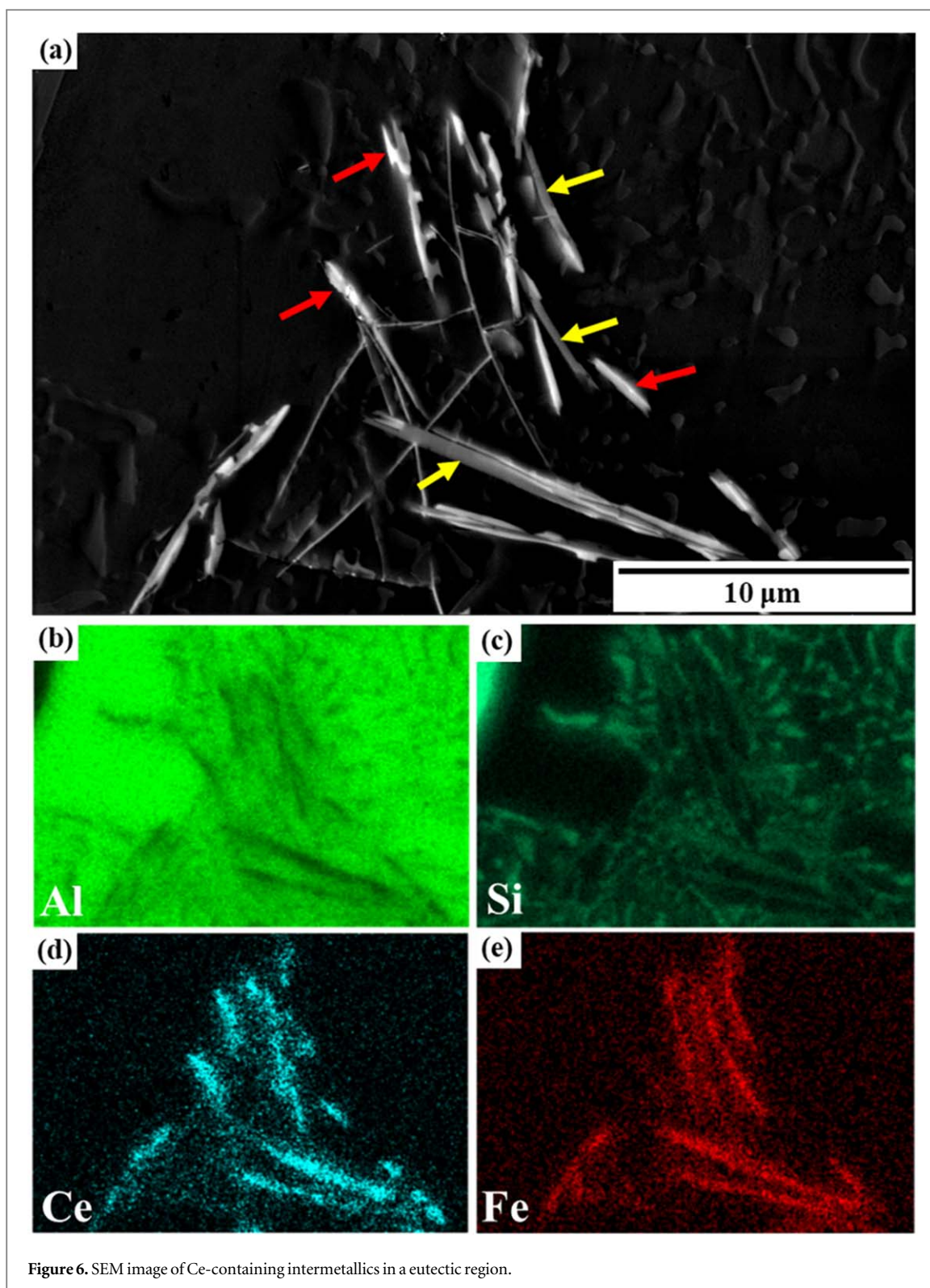
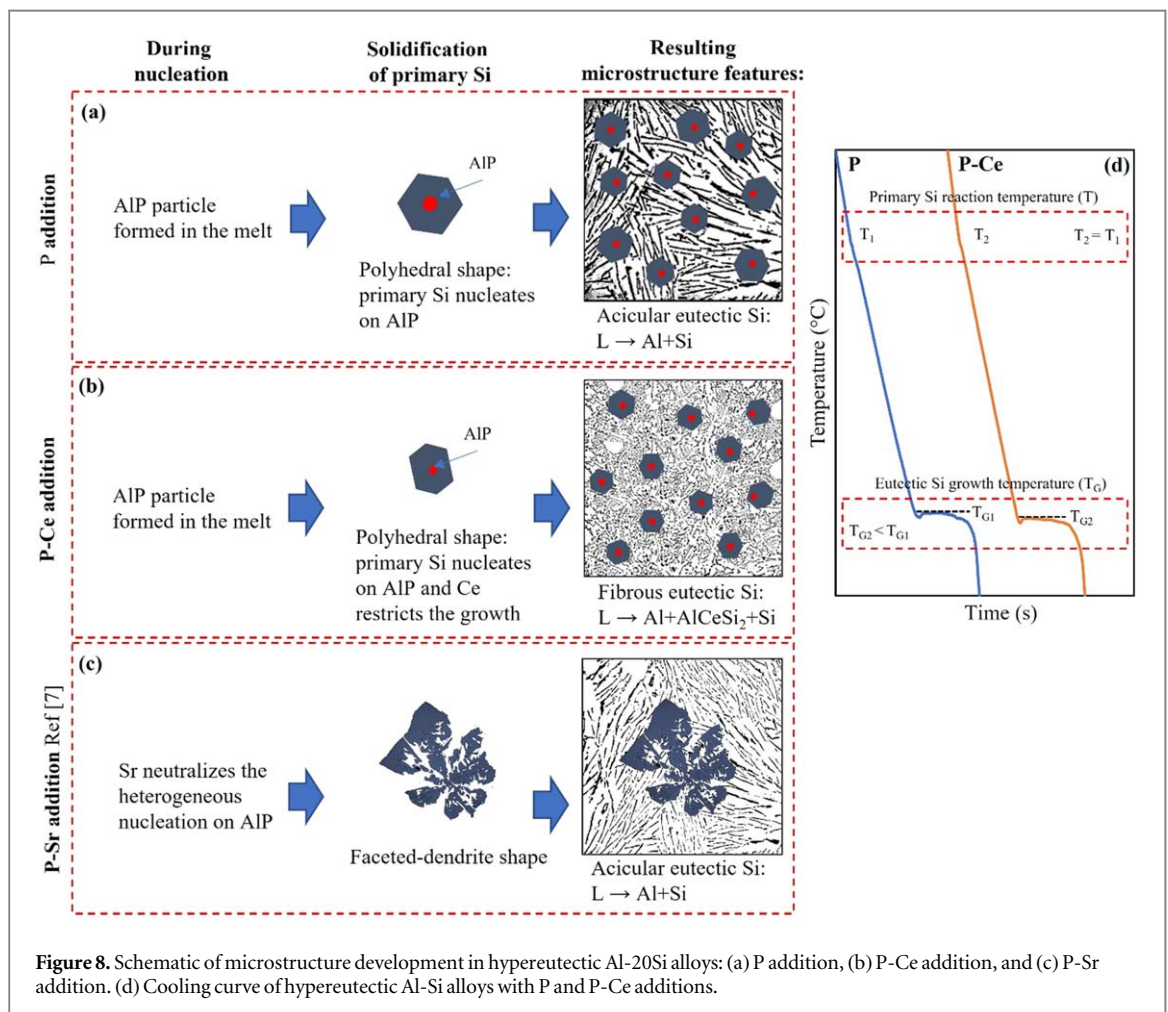
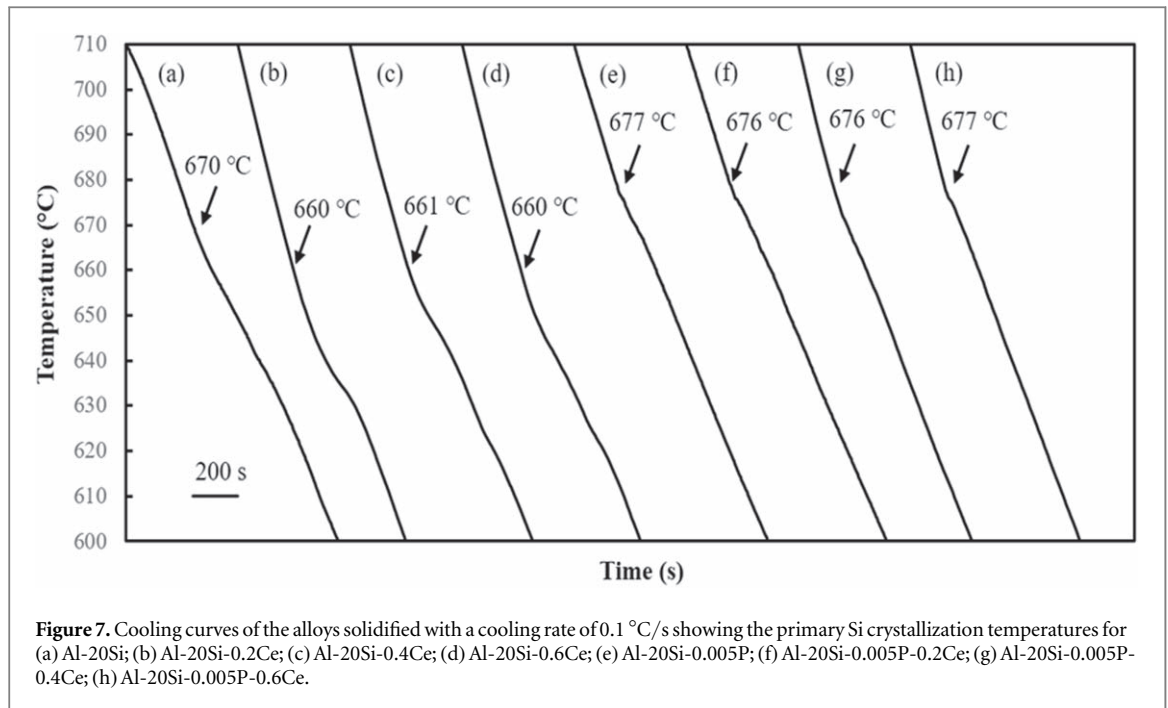


Figure 6. SEM image of Ce-containing intermetallics in a eutectic region.

intermetallic phase is present around the primary Si. The Al-Ce intermetallic phase, that is, AlCe, solidifies in the melt prior to the solidification of primary Si. However, the crystal structure and lattice parameter of AlCe correspond to those of an orthorhombic system [24], and the large variations in the lattice parameter and crystal structure are not suitable for primary Si nucleation sites. This suggests that Ce does not exhibit a distinctive nucleation function.

The primary Si refinement in hypereutectic Al-Si alloys by Ce is related to a decrease in the nucleation temperature [25] and the limited growth caused by a decrease in the growth temperature. Therefore, the diffusion rate was reduced [13]. However, the results show that the primary Si reaction temperature does not change significantly with the addition of Ce (figure 7). Ce is enriched at the solid/liquid interface during the



solidification of the casting and attracts Si solute atoms to form intermetallic compounds. The formation of Al-Si-Ce intermetallic compounds in Al-Si-Ce alloys has been reported [26]. Ce-containing intermetallic compounds are formed in the melt, which restrict the growth of primary Si.

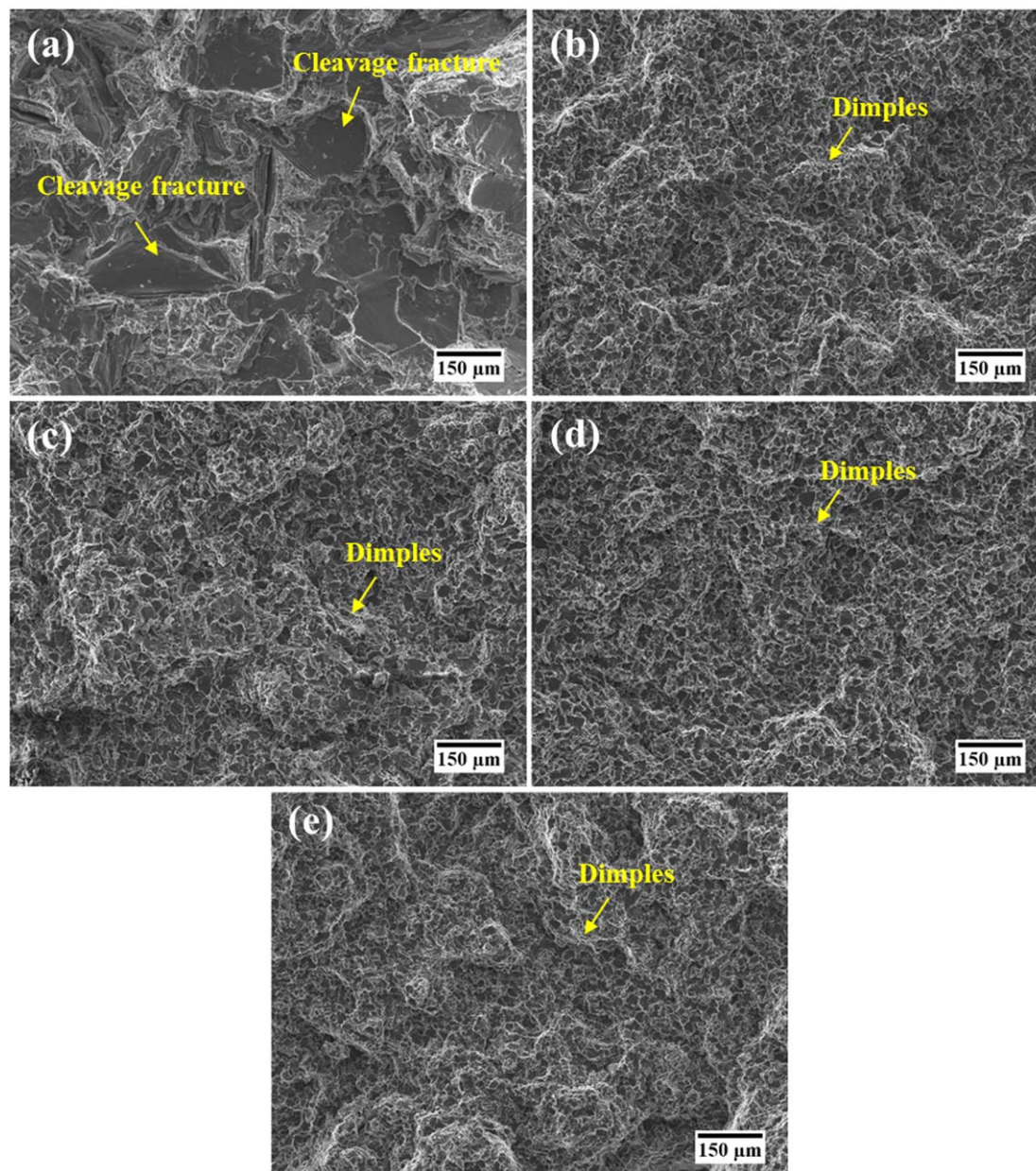


Figure 9. SEM fractographs of the tensile samples of the studied alloys: (a) Al-20Si; (b) Al-20Si-0.005P; (c) Al-20Si-0.005P-0.2Ce; (d) Al-20Si-0.005P-0.4Ce; (e) Al-20Si-0.005P-0.6Ce.

Our previous study showed that Sc decreases the efficiency of P refinement owing to the formation of ScP in hypereutectic Al-Si alloys [15]. However, intermetallic phases containing both Ce and P were not observed. We suggest that P is consumed during the formation of AlP, and therefore, a less or negligible amount of CeP is formed. In this study, it can be concluded that AlP is not affected by the interaction between Ce and P.

Many studies have reported that the refinement mechanism of primary and eutectic Si can be explained using the restricted growth theory. The restricted growth theory assumes that atoms of the modifier adsorb on the TPRES sites of growing Si crystals and inhibit the attachment of Si atoms during Si growth [21]. Furthermore, the impurity-induced twinning (IIT) mechanism produces more twin formation [27], and larger undercooling occurs during solidification. Consequently, the eutectic Si phase has a higher tendency to grow isotropically with a fine fibrous structure. Prior research indicates that the ratio of the atomic radii for potent modifiers, including Sr [28] and Eu [29], is ~ 1.65 , as predicted by the IIT theory [27]. The modifiers were segregated and consistently distributed within the fibrous Si phase in the modified alloys. For Ce, the $r_{\text{Ce}}/r_{\text{Si}}$ ratio is ~ 1.56 [27], which is close to the ideal r/r_{Si} ratio (1.65) for the modification of eutectic Si via the IIT mechanism. Therefore, the modification of eutectic Si with Ce can be explained using the absorption theory.

Another factor that might affect Al-Si eutectic growth is the formation of Al-Si-Ce intermetallic phases, as shown in figure 6. Previous studies on Al-Si-Ce alloys revealed that only two phases of Ce ($\tau_1 = \text{Ce}(\text{Si}_{1-x}\text{Al}_x)_2$ or

Table 1. Tensile properties of the experimental alloys (with standard deviations in square brackets).

Alloys	As-cast		
	UTS (MPa)	YS (MPa)	El (%)
Al-20Si	96 [3]	82 [6]	1.0 [0.4]
Al-20Si-0.005P	160 [1]	124 [1]	1.5 [0.2]
Al-20Si-0.005P-0.2Ce	163 [4]	124 [2]	1.9 [0.1]
Al-20Si-0.005P-0.4Ce	164 [4]	131 [2]	1.6 [0.3]
Al-20Si-0.005P-0.6Ce	175 [3]	136 [4]	1.7 [0.4]

$\tau_2 = \text{AlCeSi}_2$) were stable at low Ce concentrations [26]. The stable Al-Si-Ce intermetallic phase is allowed to form in the reaction $\text{L} \rightarrow \text{Al} + \text{AlCeSi}_2 + \text{Si}$ at 568.7 °C [30]. Similar to the formation of Al-Si-Ce phases, the formation of AlSi_2Sc_2 [31] and $\text{Al}_2\text{Si}_2\text{Yb}$ [32] phases was observed within the eutectic Si. This additional Al-Si-Ce phase in the eutectic, which alters solute rejection at the solid/liquid front, possibly affects the eutectic Si morphology. Therefore, Ce was effective for the simultaneous refinement of primary and eutectic Si.

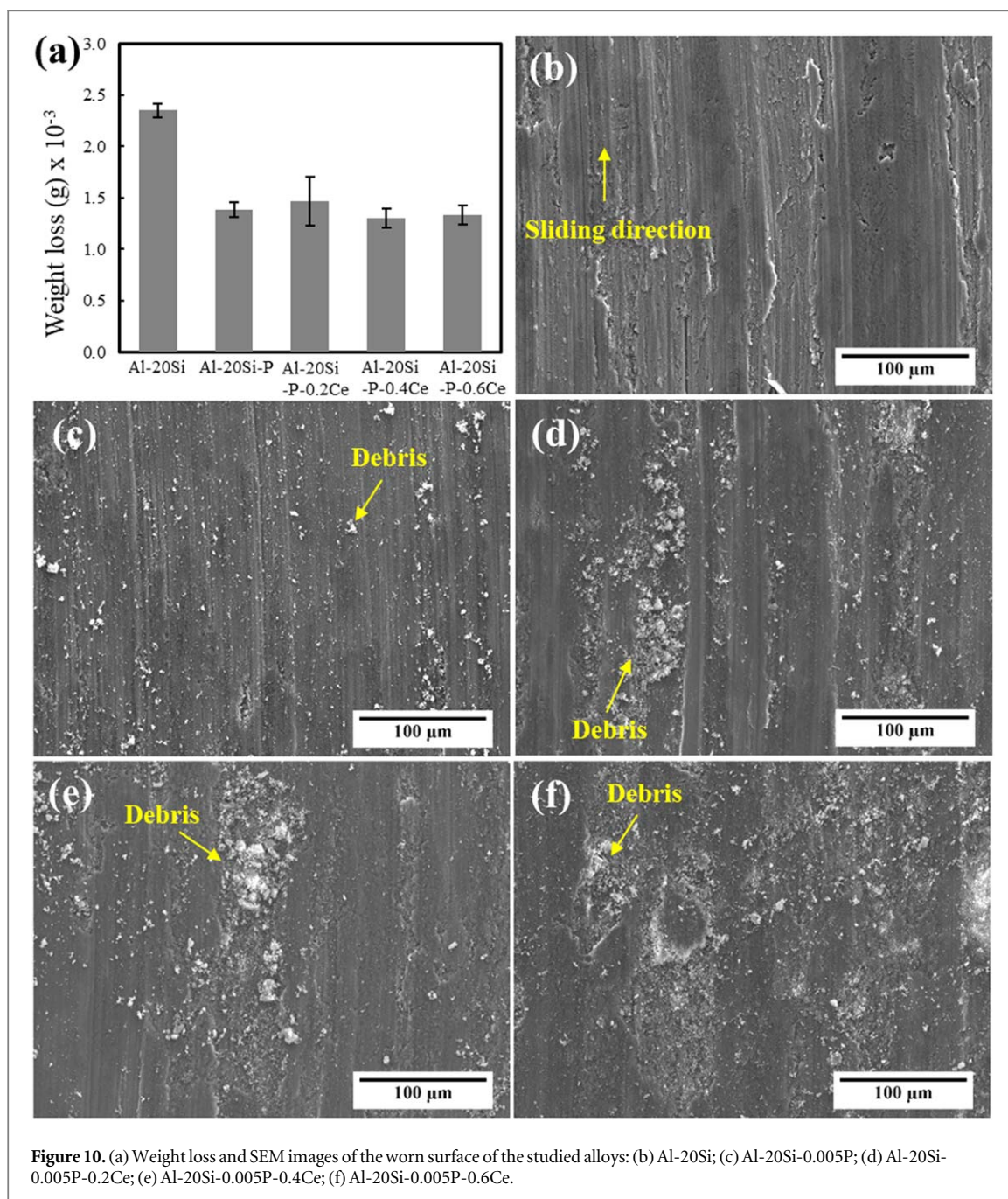
When Sr is used together with P to modify eutectic Si, Sr combines with P to form strontium-phosphide, which is more stable than AlP. Therefore, Sr neutralizes the effect of added P in refining the primary Si [7]. Consequently, the addition of P-Sr coarsens the primary Si crystals and deteriorates their mechanical properties. The addition of P-Ce is an alternative method for achieving the simultaneous refinement of primary and eutectic Si.

Figure 8 is a schematic of the microstructure formation in hypereutectic Al-20Si alloys. After P is added (figure 8(a)), the AlP particle forms in the melt at a high temperature. AlP particles are potent nuclei for primary Si formation because of the excellent lattice match between AlP and Si. Therefore, primary Si with a polyhedral shape is formed via heterogeneous nucleation. However, the eutectic Si remains acicular-like. When P and Ce are added to the melt (figure 8(b)), the AlP particle functions as a heterogeneous nucleation site for primary Si. Moreover, the primary Si is further refined by Ce owing to Ce solute enrichment at the solid/liquid interface during solidification, restricting the growth of primary Si. In addition, Ce changes the eutectic reaction from $\text{L} \rightarrow \text{Al} + \text{Si}$ to $\text{L} \rightarrow \text{Al} + \text{AlCeSi}_2 + \text{Si}$ at 568.7 °C (figure 8(d)), which affects the eutectic Si morphology. The eutectic Si is transformed from an acicular-like to a fibrous morphology owing to the addition of Ce. When compared with the structures obtained via the conventional addition of P-Sr (figure 8(c)), which is a commercial alloying element, the primary Si in this study is less faceted and more dendritic because of the restricting nucleant particles causing the slight refinement of the eutectic Si [7].

3.3. Tensile properties

The microstructure analysis reveals that the addition of Ce to the Al-20Si alloy non-uniformly refined the primary Si crystal; therefore, the mechanical properties of the Ce-refined Al-20Si alloy may deteriorate. Tensile and wear tests were performed on five sets of the following alloys: Al-20Si, Al-20Si-0.005P, Al-20Si-0.005P-0.2Ce, Al-20Si-0.005P-0.4Ce, and Al-20Si-0.005P-0.6Ce. The tensile properties of the as-cast Al-20Si alloys with and without the addition of P and Ce are presented in table 1. The Al-20Si alloy has a UTS, YS, and %El values of 96 MPa, 82 MPa, and 1.0%, respectively. The addition of P enhanced the UTS, YS, and %El by approximately 60, 50, and 40%, respectively (UTS = 160 MPa, YS = 124 MPa, and 1.5%El). The addition of 0.2 wt% Ce to the P-refined Al-20Si alloy caused slight increases in the UTS, YS, and %El. Moreover, further additions of 0.4 and 0.6 wt% Ce enhanced the tensile properties. The Al-20Si-0.005P-0.6Ce alloy had a UTS, YS, and %El of 175 MPa, 136 MPa, and 1.7%, respectively. To investigate the fracture behavior, several tensile specimens were selected for fractographic examination using SEM, as shown in figure 9. Many irregular cleavage planes were apparent on the entire fracture surface of the Al-20Si alloy without P-Ce (figure 9(a)). Figures 9(b)–(e) show that the fracture surface comprised dimples, suggesting ductile fracture due to the addition of P-Ce.

The tensile properties strongly depend on both the morphology and size of the primary and eutectic Si. The presence of coarse, irregularly shaped primary Si particles (figure 1(a)) leads to brittle fractures. Moreover, cracks are initiated and propagated along the primary Si particle/Al matrix interfaces, and the neighboring cracks link and cause material fracture. Coarse irregular primary Si and needle-like eutectic Si present sharp edges or ends, which are stress concentration sites and are susceptible to crack initiation. Therefore, the refinement of primary Si and modification of the eutectic Si structure by adding P-Ce to the Al-20Si alloy can improve the tensile strength and elongation. The strengthening mechanisms of rare earth elements are primarily based on microstructure refinement and second phase strengthening [33–35]. The addition of Ce in large amounts (up to 0.6 wt%) can easily lead to interactions with Fe and Si to form the Ce containing intermetallic phase, as shown in figure 6. This result is similar to the previous study that reported that Ce addition to Al-Si



alloys can modify the Fe-rich intermetallic phase, which is less detrimental to the tensile properties [36]. Furthermore, dimple fractures are evident in figures 9(b)–(e). This was associated with the increased plastic deformation caused by the addition of P-Ce, which is in agreement with the improved mechanical properties.

3.4. Wear behavior

The weight loss of the studied alloys (figure 10(a)) decreased with the addition of P-Ce. The worn surface of the Al-20Si alloy (figure 10(b)) possesses deep and wide grooves parallel to the motion direction, many dimples, and local adherent scars, which suggest that the main wear mechanism for the Al-20Si alloys involves a combination of abrasive and adhesive wear. When P is present (figure 10(c)), only a few shallow and narrow grooves are observed, representing a single mild abrasion wear. When P-Ce was present (figure 10(d)–(f)), the grooves of the Al-20Si worn surface were shallow and narrow. Moreover, the wear debris was black, indicating that it consisted of oxygen, suggesting that oxidative wear was the dominant wear mechanism.

The wear behavior of hypereutectic Al-Si alloys is related to their microstructure. The high wear resistance resulted from the presence of fine and well-dispersed hard particles. In this study, the fine primary and eutectic Si phases obtained via P-Ce addition suppressed the initiation and propagation of cracks at the interface of the primary Si/matrix, resulting in the enhanced wear resistance of hypereutectic Al-Si alloys. Moreover, the

addition of Ce to hypereutectic Al-Si alloys increases the wear resistance. The addition of up to 2 wt% Ce improves the wear resistance of the Al-12Si-4Mg alloy owing to the formation of an Al-Ce intermetallic phase [37].

4. Conclusions

In this study, the effects of P-Ce addition on the primary and eutectic Si as well as on the tensile and wear properties of a hypereutectic Al-20Si alloy were investigated. The following conclusions were drawn:

- Ce can significantly refine primary Si, such that the morphology transforms from a coarse, irregular, and star-like structure to an organized polyhedron, and its size decreases.
- Ce refinement is caused by the decrease in the primary Si solidification temperature, resulting in an increase in the mean growth velocity.
- Ce addition altered the eutectic Si morphology from a coarse, needle-like, and acicular shape to a fibrous shape.
- Ce does not react with P to form an intermetallic compound.
- The addition of P-Ce is an effective way to simultaneously refine the primary and eutectic Si.
- The refinement of the primary and eutectic Si via the addition of P-Ce improved the tensile strength. After adding 0.005 wt% P and 0.6 wt% Ce, the ultimate tensile strength of Al-20Si increased by 82%—from 96 MPa to 175 MPa, and the elongation increased by 70%—from 1.0% to 1.7%. The fracture formation undergoes a transition from brittle to ductile failure with the addition of P-Ce.
- The addition of P-Ce to the Al-20Si alloy improves its wear resistance.

Acknowledgments

The authors sincerely thank Prof. Sindo Kou (University of Wisconsin-Madison, USA) and Prof. Dmitry Eskin (Brunel University London, UK) for their useful discussions.

Data availability statement

The data generated and/or analysed during the current study are not publicly available for legal/ethical reasons but are available from the corresponding author on reasonable request.

Funding

The support for Mr Peerawit Chokemorh's PhD study from Rajamangala University of Technology Isan (Khon Kaen Campus) is highly appreciated. This study was financially supported by the Thailand Science Research and Innovation (TSRI) under the Fundamental Fund 2022 (Project: Advanced Materials and Manufacturing for Applications in New S-curve Industries).

ORCID iDs

P Chokemorh: conceptualization, methodology, investigation, and writing original draft; **P Pandee:** conceptualization, investigations, writing original draft, reviewing, and editing; **S Chankitmunkong:** investigations, reviewing, and editing; **U Patakham:** investigations and reviewing; and **C Limmaneevichitr:** conceptualization, reviewing, editing, and supervision.

ORCID iDs

Chaowalit Limmaneevichitr  <https://orcid.org/0000-0003-4776-3294>

References

- [1] Gruzleski J and Closset B 1990 The treatment of liquid aluminum-silicon alloys *American Foundrymen's Society* (Des Plaines, IL: American Foundrymen's Society)
- [2] Xu Y, Deng Y, Casari D, Mathiesen R H, Liu X and Li Y 2020 *J. Mater. Sci.* **55** 15621–35
- [3] Liang S M and Schmid-Fetzer R 2014 *Acta Mater.* **72** 41–56
- [4] Ludwig T H, Schaffer P L and Arnberg L 2013 *Metall. Mater. Trans. A* **44** 5796–805
- [5] Flood S C and Hunt J D 1981 *Metal. Sci.* **15** 287–94
- [6] Dahle A K, Nogita K, McDonald S D, Zindel J and Hogan L 2001 *Metall. Mater. Trans. A* **32** 949–60
- [7] Nogita K, McDonald S D and Dahle A K 2004 *Philos. Mag.* **84** 1683–96
- [8] Li Q, Li J, Li B, Zhu Y, Liu D, Lan Y and Wang S 2018 *J Mater. Eng. Perform.* **27** 3498–507
- [9] Bagaber S A, Abdullahi T, Harun Z, Daib N and Othman M H D 2017 *Arabian J. Sci. Eng.* **42** 4559–64
- [10] Li Q, Xia T, Lan Y, Zhao W, Fan L and Li P 2013 *J. Alloys Compd.* **562** 25–32
- [11] Lin G Y, Li K, Feng D, Feng Y P, Song W Y and Xiao M Q 2019 *Trans. Nonferrous Metal Soc. China* **29** 1592–600
- [12] Vijeesh V and Prabhu K N 2018 *J. Mater. Eng. Perform.* **27** 5656–64
- [13] Chang J, Moon I and Choi C 1998 *J. Mater. Sci.* **33** 5015–23
- [14] Weiss J and Loper C 1987 *AFS Trans.* **32** 51
- [15] Chokemorh P, Pandee P and Limmaneevichitr C 2018 *Int. J. Cast Met. Res.* **31** 269–78
- [16] Kasprzak W, Sediako D, Walker M, Sahoo M and Swainson I 2011 *Metall. Mater. Trans. A* **42** 1854–62
- [17] Li J, Hage F S, Liu X, Ramasse Q and Schumacher P 2016 *Sci. Rep.* **6** 25244
- [18] Atasoy O A, Yilmaz F and Elliott R 1984 *J. Cryst. Growth* **66** 137–46
- [19] Kobayashi K F and Hogan L M 1985 *J. Mater. Sci.* **20** 1961–75
- [20] McDonald S D, Nogita K and Dahle A K 2004 *Acta Mater.* **52** 4273–80
- [21] Lu S Z and Hellawell A 1985 *J. Cryst. Growth* **73** 316–28
- [22] Chen X, Geng H and Li Y 2006 *Mater. Sci. Eng. A* **419** 283–9
- [23] Pandee P, Gourlay C M, Belyakov S N, Ozaki R, Yasuda H and Limmaneevichitr C 2014 *Metall. Mater. Trans. A* **45** 4549–60
- [24] Czerwinski F 2020 *J. Mater. Sci.* **55** 24–72
- [25] Vijeesh V and Prabhu K N 2014 *Trans. Indian. Inst. Met.* **67** 541–9
- [26] Gröbner J, Mirković D and Schmid-Fetzer R 2004 *Metall. Mater. Trans. A* **35** 3349–62
- [27] Lu S Z and Hellawell A 1987 *Metall. Trans. A* **18** 1721–33
- [28] Nogita K, Yasuda H, Yoshida K, Uesugi K, Takeuchi A, Suzuki Y and Dahle A K 2006 *Scr. Mater.* **55** 787–90
- [29] Li J, Hage F, Wiessner M, Romaner L, Scheiber D, Sartory B, Ramasse Q and Schumacher P 2015 *Sci. Rep.* **5** 13802
- [30] Lu Z, Li X and Zhang L 2017 *J. Phase Equilib. Diffus.* **39** 57–67
- [31] Pandee P, Gourlay C M, Belyakov S A, Patakham U, Zeng G and Limmaneevichitr C 2018 *J. Alloys Compd.* **731** 1159–70
- [32] Li J H, Suetsugu S, Tsunekawa Y and Schumacher P 2013 *Metall. Mater. Trans. A* **44** 669–81
- [33] Zhai F, Wang L, Gao X, Zhao S, Feng Y, Ma T and Fan R 2021 *Mater. Res. Express* **8** 016521
- [34] Zhai F, Wang L, Gao X, Feng Y, Zhao S and Wang L 2020 *Mater. Res. Express* **7** 076518
- [35] Zhai F, Wang L, Gao X, Feng Y, Zhao S and Wang L 2021 *Trans. Indian Inst. Met.* **74** 2639–49
- [36] Fan C, Long S Y, Yang H D, Wang X J and Zhang J C 2013 *Int. J. Miner. Metall. Mater.* **20** 890–5
- [37] Anasyida A, Daud A and Ghazali M 2010 *Mater. Des.* **31** 365–74